Low-Temperature Flow Properties of Vegetable Oil/Cosolvent Blend Diesel Fuels

R.O. Dunn*

Food & Industrial Oils Research, USDA, ARS, NCAUR, Peoria, Illinois 61604

ABSTRACT: Vegetable oils are an attractive renewable source for alternative diesel fuels. However, the relatively high kinematic viscosity of vegetable oils must be reduced to make them more compatible with conventional compression-ignition engines and fuel systems. Cosolvent blending is a low-cost and easy-to-adapt technology that reduces viscosity by diluting the vegetable oil with a low-M.W. alcohol (methanol or ethanol). The cosolvent (**A**), which consists of one or more amphiphilic compounds, is added to solubilize the otherwise nearly immiscible oil–polar alcohol mixture. This work investigates cold flow properties and phase equilibrium behavior associated with blends consisting of soybean oil (SBO) and methanol where **A** = 8:1 (mol) *n*-butanol/oleyl alcohol; 6:1 (mol) 2-octanol/triethylammonium linoleate; and 4:1 (mol) 2-octanol/Unadol 40 (alcohols from SBO FA); and a blend of 2:1 (vol/vol) No. 2 diesel fuel/SBO and 95% ethanol where **A** = *n*-butanol. Cloud point (CP), pour point, cold filter plugging point (CFPP), and low-temperature flow test (LTFT) results were compared with corresponding phase separation temperature (T_ϕ) data measured at equilibrium. Although CP data were measured under non-equilibrium experimental conditions, a nearly linear correlation was found between T_ϕ and CP. Statistical analysis showed that T_ϕ may also be correlated with CFPP and LTFT. Analysis of heating and cooling DSC curves indicated that peak temperatures may be employed to predict cold flow properties and T_ϕ behavior for SBO/cosolvent blends. Cooling curve parameters correlated more readily than heating curve parameters. Finally, relatively low quantities of heat evolved during freezing indicated that crystallization in the SBO/cosolvent blends studied in this work occurs easily during cooling.

Paper no. J10179 in *JAOCS 79,* 709–715 (July 2002).

KEY WORDS: Cloud point, cold filter plugging point, cosolvency, diesel fuel, differential scanning calorimetry, low-temperature flow test, phase equilibria, pour point.

Recent cost and availability trends have led to increased emphasis on developing alternative fuels that are produced from domestic feedstocks. Consequently, interest in developing renewable vegetable oil-based fuels for combustion in compression ignition (diesel) engines has also increased.

Transesterification with simple alcohols to form monoalkyl FA esters (biodiesel) has drawn much attention as a viable technique for converting vegetable oils or animal fats into diesel fuel. Biodiesel made from soybean oil (SBO) has many fuel properties, such as kinematic viscosity, specific gravity, cetane number, and gross heat of combustion, that are comparable to those of No. 2 diesel fuel (D2). On the other hand, biodiesel has a number of disadvantages. Depending on feedstock, biodiesel has relatively poor cold flow properties, which may limit its distribution in moderate temperature climates. For example, methyl soyate has a cloud point (CP) of approximately 0°C compared with −16°C for D2 (1). Although combustion of biodiesel reduces harmful exhaust emissions including hydrocarbons, particulate matter, carbon monoxide, and polycyclic aromatic hydrocarbons, it does not greatly reduce nitrogen oxides (NO_x) emissions (2–5). Biodiesel also has an economic disadvantage because it is more costly to produce than conventional diesel fuels.

An alternative conversion technology for producing alternative diesel fuels from vegetable oils is cosolvent blending. Cosolvent blends typically consist of a mixture of vegetable oil and a low-M.W. alcohol (methanol or ethanol) stabilized by an amphiphilic cosolvent (**A**). Addition of **A** primarily promotes solubilization in otherwise nearly immiscible TAG–alcohol mixtures (6–12) and may secondarily stabilize additives designed to improve fuel properties such as cetane number and resistance to oxidation or to enhance the combustion process.

A literature review of fuel properties and diesel engine performance characteristics comparing vegetable oil/cosolvent blends, including those selected for study in this work, and conventional diesel fuels was reported earlier (13). Typically, cosolvent blends have kinematic viscosities comparable to biodiesel (14). Although SBO-based blends have relatively low cetane numbers (<40), audible engine knock during testing did not increase with respect to reference D2 (11). Despite having typically 20% lower gross heats of combustion, short-term (3.5 h) engine testing of SBO-based blends showed very little loss in power maxima (11,15). Although fuel consumption increased to compensate for the lower heats of combustion, this increase was partially mitigated by a 6% gain in thermal efficiency at full power. Sunflower oil/– and SBO/cosolvent blends have passed the 200-h Engine Manufacturer's Association durability test (15–18). Cosolvent blends were reported to produce less wear, with deposit formation attributed to incomplete combustion being similar to though not so extensive as noted following tests of neat vegetable oil (19).

Cosolvent blends and other vegetable oil mixtures are known to reduce harmful exhaust emissions, including NO_x, hydrocarbons, particulate matter, carbon monoxide, and polycyclic aromatic hydrocarbons (20–26). Similarly, alcohols

*Address correspondence at USDA/ARS/NCAUR, 1815 N. University St., Peoria, IL 61604-3999. E-mail: dunnro@ncaur.usda.gov

such as methanol and ethanol are known to reduce the temperature of combustion (27–30), a condition that can decrease NO_x, particulate matter, carbon dioxide, and smoke in exhaust emissions.

The cold flow properties of vegetable oil/cosolvent blends must be evaluated before they will be viable as alternative diesel fuel candidates. An earlier work (13) examined effects of low temperatures on SBO/cosolvent blends and reported that equilibrium phase separation temperature (T_ϕ) was influenced by **A** itself. Mixtures with an **A** designed to avert crystallization of high-m.p. fatty compounds (TAG, fatty alcohol, or fatty amine) favored phase separations driven by the relative solubility of low-M.W. alcohol (methanol). That is, such mixtures experienced phase separation into two immiscible liquid layers rather than a "CP-type" separation. Increasing **A**/oil mass ratio generally decreased T_ϕ. Kinematic viscosities of blends were comparable to methyl soyate (biodiesel) at lower temperatures.

This study investigates cold flow properties of four SBO/cosolvent blends—three SBO/**A**/methanol blends where **A** = 8:1 (mol) *n*-butanol/oleyl alcohol, 6:1 (mol) 2-octanol/triethylammonium linoleate, and 4:1 (mol) 2-octanol/Unadol 40 (alcohols derived from SBO FA); plus one blend [2:1 (vol/vol) D2/SBO]/**A**/95 wt% ethanol (E95; 5% aqueous) where **A** = *n*-butanol. Results from T_ϕ measurements were analyzed for correlation with cold flow properties CP, pour point (PP), cold filter plugging point (CFPP), and low-temperature flow test (LTFT). In addition, heating and cooling DSC curves were analyzed for prediction of cold flow properties and T_ϕ.

EXPERIMENTAL PROCEDURES

Materials. Bleached, alkali-refined SBO (density at 25°C = 0.912 g/mL) was from Archer Daniels Midland, Inc. (Decatur, IL). The FA profile was as reported earlier (13). Technical grade oleyl alcohol [65 wt% 9(*Z*)-octadecen-1-ol] and 2-octanol (98%) were from Aldrich (Milwaukee, WI). Unadol 40 [54% 9(*Z*),12(*Z*)-octadecadien-1-ol] was from Sherex (New York, NY). Emersol 315 [59.0% 9(*Z*),12(*Z*)-octadecenoic acid] was from Emery Industries (Cincinnati, OH). Triethylamine (99+%) was from Sigma (St. Louis, MO). Analytical grade methanol (99+%) was from EM Science (Gibbstown, NJ), E95 from Millennium Petrochemicals, Inc. (Iselin, NJ), and *n*-butanol (99.8 %) from Fisher Scientific (Pittsburgh, PA). When not in use, methanol, *n*-butanol, and 2-octanol were stored over 4Å molecular sieves from Union Carbide (Danbury, CT). Low-sulfur (<0.05 wt%) Phillips standard D2 was provided by the National Institute for Petroleum and Energy Research (Bartlesville, OK).

Methods. Methods for mixing cosolvent blends and measurement of T_ϕ data (±0.5°C) were reported earlier (13). For System III mixtures (see Table 1), equimolar proportions of triethylamine and Emersol 315 were mixed in solution with SBO prior to blending with methanol.

Low-temperature filterabilities were measured in accordance with corresponding ASTM standard methods (see below). Apparatus for measuring CP, PP, and CFPP were from Koehler (Bohemia, NY); apparatus for measuring LTFT was constructed in-house as reported earlier (1).

Heating and cooling DSC analyses were carried out with a TA Instruments, Inc. (New Castle, DE) model 2910 DSC with a model 2100 PC-based controller. The measurement cell was purged with low-pressure nitrogen gas and fitted with a liquid nitrogen-cooled heat exchanger for subambient analyses. Approximately 10 mg of sample was hermetically sealed in an aluminum pan and scanned with respect to an empty reference pan. For heating scans, samples were cooled and held isothermally at −100°C for 10 min before ramping to 40°C at 5°/min. For cooling scans, samples were equilibrated at 30°C then cooled at 5°/min to −100°C.

RESULTS AND DISCUSSION

Table 1 is a list of oil, **A**, and alcohol components used to formulate the cosolvent blends investigated in this work. The term System *m*, where *m* = I, II, III, or V, refers to an oil/**A**/alcohol blend with arbitrary composition. The term FS#*n*, where *n* = 1, 2, 3, or 5, refers to a blend with a singular composition as defined in Table 2.

Cold flow properties of SBO/cosolvent blends. Cold flow properties for FS#1, FS#2, FS#3, FS#5, neat SBO, and a 2:1 (vol/vol) D2/SBO mixture are listed in Table 3. These results were consistent with the following trends: (i) CP > PP (exception: CP = PP for D2/SBO); (ii) LTFT > CFPP; (iii) CP > CFPP, LTFT > PP (exceptions: FS#5, where CFPP < PP; SBO, where CFPP, LTFT > CP).

For the D2/SBO mixture, SBO dominates the crystalline nucleation and growth mechanisms that determine CP and PP. CP is determined by cooling the sample and checking visually at 1°C intervals for a cloud-like suspension. The temperature at which particles are detected is the measured CP (31). In contrast, PP is determined by cooling the sample and

TABLE 1
Oil/Cosolvent (A)/Alcohol Reference System Components[a]

System	Oil	**A**	Alcohol
I	SBO	1:8 (mol) oleyl alcohol/*n*-butanol	Methanol
II	SBO	1:6 (mol) triethylammonium linoleate[b]/2-octanol	Methanol
III	SBO	1:4 (mol) Unadol 40/2-octanol	Methanol
V	2:1 (vol/vol) D2/SBO	*n*-butanol	E95

[a]D2 = low-sulfur (0.05 wt%) No. 2 diesel fuel; E95 = 5 wt% aqueous (190 proof) ethanol; SBO = soybean oil; Unadol 40 = fatty alcohols derived from SBO FA.
[b]Prepared from equimolar portions of triethylamine and Emersol 315 (soy FA) mixed in SBO.

TABLE 2
Compositions of Selected Oil/A/Alcohol Blends[a]

Solution	System	Composition (mass frac.)	**A**/oil (g/g)
FS#1	I	SBO (0.400) Oleyl alcohol (0.111) *n*-Butanol (0.250) Methanol (0.239)	0.902
FS#2	II	SBO (0.307) Triethylammonium linoleate (0.128) 2-Octanol (0.246) Methanol (0.319)	1.218
FS#3	III	SBO (0.415) Unadol 40 (0.115) 2-Octanol (0.223) Methanol (0.247)	0.814
FS#5	V	D2 (0.497) SBO (0.267) *n*-Butanol (0.189) E95 (0.047)	0.247

[a]FS#*n* = cosolvent blend derived from corresponding reference system (see Table 1). See Table 1 for other abbreviations.

TABLE 3
Equilibrium Phase Separation Temperature (T_ϕ) and Low-Temperature Flow Properties of Selected Cosolvent Blends[a]

Solution[b]	CP[c] (°C)	PP (°C)	LTFT (°C)	CFPP (°C)	T_ϕ (°C)
FS#1	+5	–26	–7	–16	–0.5
FS#2	+5	–24	–3	–21	1.5
FS#3	–8	–16	–5	–14	–3.5
FS#5	–16	–19	–15	–24	–16
SBO	–6	–11	+14	+11	–4
2:1 (vol/vol) D2/SBO	–18	–18	–17	–21	—

[a]CFPP, cold filter plugging point; CP, cloud point; LTFT, low-temperature flow test; PP, pour point; T_ϕ, equilibrium phase separation temperature. See Table 1 for other abbreviations.
[b]Solutions FS#1, FS#2, FS#3, and FS#5 were prepared as defined in Table 2.
[c]CP, PP, and CFPP data are mean values from three replicate measurements; variance ≤0.33.

checking at 3°C intervals for movement by tilting the sample container. The PP is reported as the highest temperature where movement is detected (32); that is, PP is typically 3°C warmer than the last temperature checked. Thus, if the rates of crystalline growth and agglomeration are relatively fast, it is possible the measured PP will be equal to (or 1–2°C greater than) the CP of the same sample. This was likely the case for D2/SBO in Table 3.

The CFPP is determined by cooling the fluid and measuring its flow rate through a wire mesh screen filter. The cooling rate is dictated by the surrounding bath temperature, which is set 10–25°C below the expected temperature measurement range. This test consists of placing a sample volume = 20 mL under a 0.02 atm vacuum and passing it through a 45-μm wire mesh filter. If the fluid passes the test, the process is repeated in 1°C intervals until it fails. The CFPP is the highest temperature at which the fluid fails to completely flow through the filter within 60 s (33). Strict adherence to criteria for reporting CFPP and PP could theoretically result in CFPP of a fluid being 3–4°C lower than its corresponding PP. This was likely the case for FS#5, which gave a CFPP 5°C lower than its PP.

Although apparatus and procedures are similar to those for measuring CFPP, LTFT is determined under more stringent conditions. This test consists of placing a 200 mL sample volume under a 0.2 atm vacuum and passing at least 180 mL through a 17-μm wire mesh filter. Cooling rate is 1°C/h and filterability is tested in 1°C intervals. The LTFT is the lowest temperature at which a fluid successfully passes the filter within 60 s (34). Owing to the more rigorous experimental conditions, LTFT typically occurs at higher temperatures than CFPP. Thus, it is less likely LTFT will occur at temperatures below the measured PP of a given fluid. This was the case for the solutions studied in this work.

The kinematic viscosity of neat SBO increases from 32.8 mm^2/s at 40°C to 188 mm^2/s at 0°C (13). Consequently, at temperatures in the range of 10–15°C a relatively high resistance to flow prevented SBO from easily passing either filterability test. Therefore, for neat SBO, CFPP = +11°C and LTFT = +14°C were significantly higher than its CP.

Comparison of T_ϕ *with CP*. Results listed in Table 3 show that cosolvent blends with lower T_ϕ values have lower corresponding CP values. As reported earlier (13), SBO/cosolvent blends FS#1, FS#2, and FS#3 each have T_ϕ values similar to that of neat SBO. On the other hand, whereas CP values were significantly higher for FS#1 and FS#2 than for neat SBO, CP values for FS#3 and FS#5 were within 2°C of their corresponding neat oils (SBO and D2/SBO).

The temperature at which cloud formation occurs in a given cosolvent blend may be characterized as a phase separation temperature. Similar to CFPP, CP is determined for samples cooled by setting the bath temperature 10–25°C below the expected temperature range for measurement (31), then checking visually for formation of a cloudlike suspension. Thus, CP is measured under nonsteady-state conditions rather than at equilibrium.

In contrast, T_ϕ values were measured by setting the cooling bath temperature and holding it constant during equilibration. Following equilibration, samples were withdrawn from the bath, slightly agitated, and checked visually for phase separation. The results in Table 3 show that cooling conditions influence the temperature of phase separation (T_ϕ or CP) more significantly for FS#1 and FS#2 than for FS#3 or FS#5.

Similarities between T_ϕ and CP values for Systems III and V are shown graphically in Figure 1. As the **A**/oil mass ratio increases with respect to constant methanol concentration for System III, both T_ϕ and CP decrease, showing very little deviation with respect to each other. Increasing the **A**/oil mass ratio also decreased T_ϕ and CP for System V, although the most significant decrease occurred for ratios <0.3 g/g. Statistical comparison of paired-two sample means indicated a good probability (0.342) that T_ϕ was correlated with respect to CP for System III and a very high probability (0.873) that the parameters were correlated for System V.

Figure 2 is a demonstration of how (CP, T_ϕ) data pairs could be correlated for the SBO/cosolvent blends with varying

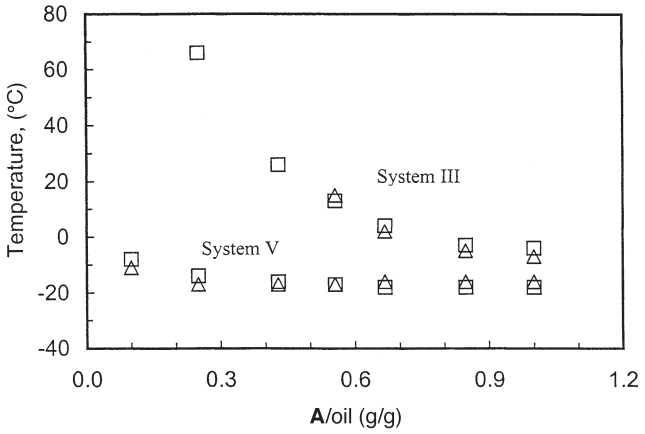

FIG. 1. Comparison of T_ϕ and CP for reference Systems III and V (see Table 1) with respect to increasing **A**/oil mass ratio. □, T_ϕ; △, CP. Methanol concentration = 0.25 g/g solution for System III; E95 concentration = 0.05 g/g solution for System V. T_ϕ, equilibrium phase separation temperature; CP, cloud point; **A**, amphiphilic cosolvent; oil: SBO for System III and 2:1 (vol/vol) No. 2 diesel fuel/soybean oil (SBO); E95, 95% ethanol.

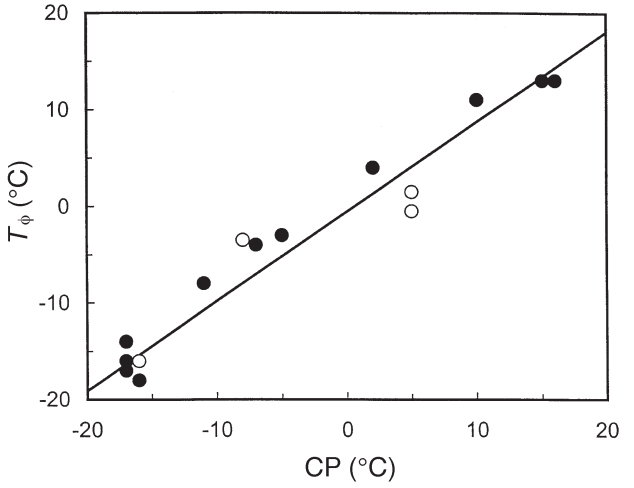

FIG. 2. Correlation between T_ϕ and CP data for several SBO/cosolvent blends based on Systems I, II, III, and V (defined in Table 1) with varying oil/**A**/alcohol compositions (●). Blends FS#1, FS#2, FS#3, and FS#5 (oil/**A**/alcohol compositions specified in Table 2) are represented by open symbols (○). For abbreviations see Figure 1.

composition derived from Systems I, II, III, and V. Least-squares linear regression analysis yielded the following equation:

$$T_\phi = 0.93(\text{CP}) - 0.5 \quad [1]$$

where the regression coefficient (R^2) = 0.93 and SE of the *y*-estimate = 2.7. The R^2 value indicates that correlation between T_ϕ and CP may not necessarily be linear. Two of the outlier points were for FS#1 and FS#2 (open symbols at CP = 5°C). Omission of these points increased R^2 to 0.96. Although this increase was significant, it is not enough to rule out a nonlinear correlation between T_ϕ and CP. Nevertheless, Equation 1 may be used to estimate T_ϕ from CP to within 3°C.

Comparison of T_ϕ *with cold flow properties*. Results in Table 3 show that T_ϕ data for FS#1, FS#2, and FS#3 were within 0.5–5.5°C of the T_ϕ for neat SBO. Only FS#3 showed a similar pattern for corresponding CP and PP data. For FS#5, CP, PP, CFPP, and LTFT data were within 1–3°C of corresponding data for its neat oil, 2:1 (vol/vol) D2/SBO. These results show that cold flow properties of oil/**A**/alcohol blends resemble those of their corresponding oil component.

Statistical comparison of T_ϕ *vs.* CP, PP, CFPP, and LTFT data for FS#1, FS#2, FS#3, FS#5 (two samples), neat SBO (two samples), and 2:1 (vol/vol) D2/SBO was conducted by analysis of paired two-sample *t*-tests. The results are summarized in Table 4.

Comparison of (CP, T_ϕ) data pairs yielded a two-tailed probability (P) = 0.658 that these parameters were correlated. This result is distinguished from those discussed individually for Systems III and V in the preceding section because results in Table 4 correspond to observations taken collectively across the four cosolvent blend solutions (defined in Table 2) plus the neat oils. Comparison of (CFPP, T_ϕ) and (LTFT, T_ϕ) data pairs yielded analogous results (P = 0.322 and 0.232). Hence, these results show that T_ϕ can be correlated with respect to CP, CFPP, or LTFT.

Statistical analysis showed very little likelihood that T_ϕ was correlated with PP, with respect to the cosolvent blends studied in this work. This was not unexpected because conditions for measuring PP necessitate that the crystalline growth and agglomeration processes be well established, such as decreasing temperature below the CP or T_ϕ of the solution.

DSC heating and cooling curve parameters. Results from analysis of DSC heating and cooling curves are listed in Tables 5 and 6. Parameters in these tables are mean values determined from replicate scans at ramp rate = 5°C/min.

In general, completion of melt (COM) temperatures determined from heating curves of SBO/cosolvent blends were influenced by the melting characteristics of their corresponding oil component. FS#1, FS#2, and FS#3 had COM values within 5.7–7.0°C of the COM of neat SBO. Although the COM of FS#5 did not compare well to that of its oil component [2:1 (vol/vol) D2/SBO], ANOVA indicated a fair comparison with the COM of neat D2 (P = 0.05). Thus, D2 may be the dominant solvent in System V at low temperatures.

Crystallization onset temperatures from the cooling curves of SBO/cosolvent blends (Table 6) were also driven by the crystallization characteristics of their corresponding oil. The

TABLE 4
Statistical Comparison of T_ϕ with Respect to Cold Flow Properties[a]

Property	*n*	Pooled variance	*t*-Value	*P*
CP	8	67	0.462	0.658
PP	8	42	–3.179	0.016
CFPP	8	139	1.066	0.322
LTFT	8	109	1.310	0.232

[a]*n*, number of observations (data pairs); *t*-value, calculated with respect to *n* and pooled variance; *P*, two-tailed probability, calculated with respect to critical *t*-value = 1.895. See Table 3 for other abbreviations.

TABLE 5
DSC Analysis of Oils and Oil/A/Alcohol Blends: Heating Curve Parameters[a]

Solution[b]	COM (°C)	Peak temperatures[c] (°C)	ΔH_m (J/g)
FS#1	10.18 ± 0.27	**–26.0**; –15.51; –0.36; 5	–1.2 ± 0.2
FS#2	9.5 ± 1.2	–64; –41.1; **–15.25**; –0.38; 7.7	–2.9 ± 0.4
FS#3	8.9 ± 0.6	–57; **–36.4**; –16.6; –0.3; 6.93	–1.9 ± 0.8
FS#5	–3.67 ± 0.45	**–26.71**; –4	0.4 ± 0.3
SBO	3.21 ± 0.25	–37.47; **–24.1**	–56 ± 2
D2	–5.5 ± 0.6	**–26**; –16; –7.3	–0.7 ± 0.2
2:1 (vol/vol) D2/SBO	6 ± 2	**–25.9**; –0.22; 4	–2.2 ± 0.8

[a]Results are from three replicate scans at 5°C/min. COM, completion of melt; ΔH_m, heat of melting of peak with warmest peak temperature. See Table 1 for other abbreviations.
[b]Solutions FS#1, FS#2, FS#3, and FS#5 were prepared as defined in Table 2.
[c]Mean values from three replicate measurements; variance = 0.0001–4.9 except at lowest peak temperature for FS#2 (11) and FS#3 (14). Peak temperatures in boldface type had the largest heats of melting.

TABLE 6
DSC Analysis of Oils and Oil/A/Alcohol Blends: Cooling Curve Parameters[a]

Solution[b]	Onset (°C)	Peak temperature[c] (°C)	ΔH_f (J/g)
FS#1	–14.54 ± 0.21	–16.28 ± 0.38	1.4 ± 0.2
FS#2	–19.5 ± 1.3	–21.7 ± 1.3	0.5 ± 0.5
FS#3	–13.60 ± 0.17	–15.63 ± 0.39	7.7 ± 0.8
FS#5[d]	–11.61 ± 0.13	–13.25 ± 0.01	0.18 ± 0.07
SBO[e]	–12.2 ± 0.6	–13.8 ± 0.5	6.0 ± 0.6
D2	–4.8 ± 0.7	–6 ± 2	0.20 ± 0.02
2:1 (vol/vol) D2/SBO	–5 ± 2	–7 ± 2	0.17 ± 0.04

[a]Results from three replicate scans at 5°C/min. Onset, crystallization onset temperature; ΔH_f, heat of fusion of highest peak. See Tables 1 and 5 for other abbreviations.
[b]Solutions FS#1, FS#2, FS#3, and FS#5 were prepared as defined in Table 2.
[c]Highest crystallization peak temperature.
[d]Onset temperature, peak temperature, and ΔH_f from two replicates.
[e]Onset and peak temperature from seven replicates; ΔH_f from four replicates.

SBO content was higher for FS#1 (0.400 g SBO/g solution, see Table 2) and FS#3 (0.415) than FS#2 (0.307). Consequently, deviations between onset temperatures were less for FS#1 (2.3°C) and FS#3 (1.4°C) than for FS#2 (7.3°C), relative to neat SBO. On the other hand, the onset for FS#5 compared better with the onset for neat SBO ($P = 0.377$) than with the onsets of neat D2 or 2:1 (vol/vol) D2/SBO.

Comparison of COM and crystallization onset temperatures provides the basis for some interesting conclusions. Heating curve analysis of the 2:1 (vol/vol) D2/SBO mixture gave a COM exceeding corresponding parameters for neat SBO and D2. Although a relatively large variance ratio ($F = 64$) precluded reliable comparison of mean values by ANOVA, the numerical difference between COM values of the D2/SBO mixture and neat SBO was less than 3°C. Thus, it is likely these results compare well with respect to each other.

ANOVA of onset data for neat D2 and 2:1 (vol/vol) D2/SBO showed a $P = 0.555$ probability these values were identical. This means it is likely that crystallization during cooling of the D2/SBO mixture was dominated by independent crystallization of D2 and SBO components rather than co-crystallization to form a homogeneous solid solution. Formation of a homogenous solid solution would have caused the onset temperature to occur more proportionately between the onsets of neat D2 and SBO.

The discrepancy between COM and crystallization onset temperature of neat SBO (15.4°C) may be due to a "tailing effect" induced by the constant ramp rate (5°C/min) during melting and/or crystallization. As noted above, SBO becomes very viscous at low temperatures, an effect that reduces self-diffusion. During melting, low self-diffusion decreases the mass transfer rate of SBO molecules from solid crystal to bulk liquid phase. In contrast, ANOVA of COM and onset temperatures of neat D2 showed a $P = 0.351$ probability that these parameters were identical, indicating no significant tailing effects induced by ramp rate.

If D2 and SBO in the D2/SBO mixture crystallize independently during cooling prior to DSC heating curve analysis, then the melting transition of SBO molecules also occurs independently of D2 molecules present in the sample. Thus, SBO crystals first melt to form "SBO-rich" liquid droplets dispersed in the bulk (mostly D2) liquid phase. In addition to the aforementioned tailing effects during melting of SBO molecules, COM of the D2/SBO mixture is affected by the rate of mass transfer of SBO molecules from SBO-rich liquid droplets to the bulk liquid phase. It is feasible that this mass transfer step, whose rate is significantly influenced by low self-diffusion of SBO molecules at low temperatures, causes COM of the 2:1 (vol/vol) D2/SBO mixture to exceed the COM results of neat SBO, although the increase is less than 3°C.

The tailing effect was also evident for the SBO/cosolvent blends, although effects were less pronounced for FS#5 than for the other three blends. For FS#1, FS#2, and FS#3, COM exceeded crystallization onset temperature by at least 21.7°C; for FS#5, COM exceeded onset by only 7.94°C. As concluded above, blends based on a 2:1 (vol/vol) D2/SBO oil component are likely to have D2 as the primary solvent at low temperatures. Therefore, dilution of SBO with D2 increases its molecular diffusion in the bulk liquid phase during cooling. Also, adding *n*-butanol improved solubilization of both SBO and E95 in FS#5, resulting in a significant decrease in COM with respect to the nonblended D2/SBO mixture (Table 5).

Finally, the heats of fusion (ΔH_f) inferred for highest-freezing peak from cooling curve analyses of the four cosolvent blends (Table 6) were relatively small (<8 J/g), suggesting that a relatively rapid phase transition occurred during crystallization in SBO/cosolvent blends at low temperatures. Similarly, the heats of melting (ΔH_m) inferred for the highest-melting peak from heating curve analysis (Table 5) were also relatively small (<–3 J/g). An exception to this trend occurred for neat SBO ($\Delta H_m = -56$ J/g) because it was the only material whose maximal-area peak was also its warmest melting peak. The cosolvent blends plus neat D2 and the D2/SBO mixture had one to three smaller peaks at temperatures above that of their maximal-area peaks. Thus, the melting and/or solvent characteristics of other components such as D2, cosolvent, and alcohol that are present affected the final transition from solid to the liquid phase.

Comparison of DSC parameters with cold flow properties and T_ϕ. Results in Table 7 indicate that parameters inferred from DSC curves may be employed to predict cold flow properties and T_ϕ data for the SBO/cosolvent blends studied in this work. Results from analysis of DSC curves were listed under Parameter 1, and cold flow properties and T_ϕ were listed under Parameter 2. Only results from *t*-test analyses of paired two-sample data favoring a correlation between corresponding parameters (that is, those showing $P > 0.10$) were listed in Table 7.

Parameters from cooling DSC curves were better suited for correlation with respect to cold flow properties and T_ϕ than were heating curve parameters. This was expected because the cold flow properties and T_ϕ data were measured with respect to continuously decreasing temperature. However, two heating curve parameters gave positive comparisons. The temperature of the heating peak with maximum area $[P(\Delta H_{max})_H]$ gave a $P = 0.175$ favoring correlation with respect to CP, whereas the next-highest melting peak temperature $[P(m-1)_H]$ was the only DSC parameter showing a correlation with respect to PP ($P = 0.116$). None of the cold flow properties nor T_ϕ could be correlated with respect to COM ($P < 0.04$), temperature of the highest (last) melting peak ($P < 0.09$), or ΔH_f of the highest (first) freezing peak ($P < 0.04$).

With the exception of PP, the other cold flow properties and T_ϕ showed a probability of correlation with respect to peak temperatures from cooling curve analyses. Crystallization onset temperature gave the best results for correlation with respect to CP ($P = 0.500$) and LTFT ($P = 0.383$). Although onset gave good results for correlation with respect to CFPP, temperature of the highest freezing peak $[P(1)_C]$ exhibited a very high probability ($P = 0.818$) of correlation. Onset had the highest probability ($P = 0.199$) for correlation with respect to T_ϕ.

ACKNOWLEDGMENTS

Dale Ehmke, Haifa Khoury, and Rebecca Zick provided technical assistance for experimental studies and analyses.

TABLE 7
Statistical Comparison of T_ϕ and Cold Flow Properties with Respect to DSC Parameters[a]

Parameter 1	Parameter 2	*n*	Pooled variance	*t*-Value	*t*-Critical	*P*
$P(\Delta H_{max})_H$	CP	7	36	1.539	1.943	0.175
$P(m-1)_H$	PP	7	90	1.834	1.943	0.116
Onset	CP	7	61	0.724	1.943	0.500
Onset	CFPP	7	84	0.600	1.943	0.571
Onset	LTFT	7	71	0.942	1.943	0.383
Onset	T_ϕ	6	38	1.478	2.015	0.199
$P(1)_C$	CP	7	62	1.046	1.943	0.336
$P(1)_C$	CFPP	7	84	0.240	1.943	0.818
$P(1)_C$	LTFT	7	72	1.277	1.943	0.249
$P(1)_C$	T_ϕ	6	38	1.874	2.015	0.120

[a] $P(\Delta H_{max})_H$, peak temperature of heating peak with largest heat of melting (peak temperature in boldface type in Table 5); $P(m-1)_H$, peak temperature of next-to-last (second-highest) melting peak; $P(1)_C$ = peak temperature of first (highest) freezing peak. See Tables 3, 4, and 6 for other abbreviations.

REFERENCES

1. Dunn, R.O., and M.O. Bagby, Low-Temperature Properties of Triglyceride-Based Diesel Fuels: Transesterified Methyl Esters and Petroleum Middle Distillate/Ester Blends, *J. Am. Oil Chem. Soc. 72*:895–904 (1995).
2. Knothe, G., R.O. Dunn, and M.O. Bagby, Biodiesel: The Use of Vegetable Oils and Their Derivatives as Alternative Diesel Fuels, in *Fuels and Chemicals from Biomass,* ACS Symp. Ser. No. 666, edited by B.C. Saha and J. Woodward, American Chemical Society, Washington, DC, 1997, pp. 172–208.
3. Chang, D.Y.Z., J.H. Van Gerpen, I. Lee, L.A. Johnson, E.G. Hammond, and S.J. Marley, Fuel Properties and Emissions of Soybean Oil Esters as Diesel Fuel, *J. Am. Oil Chem. Soc. 73*:1549–1555 (1996).
4. Krahl, J., A. Munack, M. Bahadir, L. Schumacher, and N. Elser, Survey about Biodiesel Exhaust Emissions and Their Environmental Effects, in *Proceedings of the Third Liquid Fuel Conference: Liquid Fuel and Industrial Products from Renewable Resources*, edited by J.S. Cundiff, E.E. Gavett, C. Hansen, C. Peterson, M.A. Sanderson, H. Shapouri, and D.L. Van Dyne, American Society of Agricultural Engineers, St. Joseph, MI, 1996, pp. 136–148.
5. Ali, Y., and M.A. Hanna, Alternative Diesel Fuels from Vegetable Oils, *Bioresource Technol. 50*:153–163 (1994).
6. Dunn, R.O., and M.O. Bagby, Solubilization of Methanol and Triglycerides: Unsaturated Long-Chain Fatty Alcohol/Medium-Chain Alkanol Mixed Amphiphilic Systems, *J. Am. Oil Chem. Soc. 71*:101–108 (1994).
7. Dunn, R.O., A.W. Schwab, and M.O. Bagby, Solubilization and Related Phenomena in Nonaqueous Triolein/Unsaturated Long Chain Fatty Alcohol/Methanol Solutions, *J. Dispersion Sci. Technol. 14*:1–16 (1993).
8. Dunn, R.O., A.W. Schwab, and M.O. Bagby, Physical Property and Phase Studies of Nonaqueous Triglyceride/Unsaturated Long Chain Fatty Alcohol/Methanol Systems, *Ibid. 13*:77–93 (1992).
9. Schwab, A.W., M.O. Bagby, and B. Freedman, Preparation and Properties of Diesel Fuels from Vegetable Oils, *Fuel 66*:1372–1378 (1987).
10. Schwab, A.W., and E.H. Pryde, Triglyceride-Methanol Microemulsions, *J. Dispersion Sci. Technol. 6*:563–574 (1985).
11. Goering, C.E., A.W. Schwab, R.M. Campion, and E.H. Pryde, Soyoil–Ethanol Microemulsions as Diesel Fuel, *Trans. ASAE 26*:1602–1607 (1983).
12. Schwab, A.W., H.C. Nielsen, D.D. Brooks, and E.H. Pryde, Triglyceride/Aqueous Ethanol/1-Butanol Microemulsions, *J. Dispersion Sci. Technol. 4*:1–17 (1983).
13. Dunn, R.O., and M.O. Bagby, Low-Temperature Phase Behavior of Vegetable Oil/Co-Solvent Blends as Alternative Diesel Fuels, *J. Am. Oil Chem. Soc. 77*:1315–1323 (2000).
14. Dunn, R.O., G. Knothe and M.O. Bagby, Recent Advances in the Development of Alternative Diesel Fuel from Vegetable Oils and Animal Fats, *Recent Res. Develop. Oil Chem. 1*:31–56 (1997).
15. Goering, C.E., in Final Report for Project on Effect of Nonpetroleum Fuels on Durability of Direct-Injection Diesel Engines Under Contract 59-2171-1-6-057-0, USDA, ARS, Peoria, 1984.
16. Schwab, A.W., and E.H. Pryde, Microemulsions from Vegetable Oil and Lower Alcohol with Octanol Surfactant as Alternative Fuel for Diesel Engines, U.S. Patent 4,557,734 (1985).
17. Goering, C.E., and B. Fry, Engine Durability Screening Test of a Diesel Oil/Soy Oil/Alcohol Microemulsion, *J. Am. Oil Chem. Soc. 61*:1627–1632 (1984).
18. Ziejewski, M., K.R. Kaufman, A.W. Schwab, and E.H. Pryde, Diesel Engine Evaluation of a Nonionic Sunflower Oil-Aqueous Ethanol Microemulsion, *Ibid. 61*:1620–1626 (1984).
19. Ryan, T.W., III., L.G. Dodge, and T.J. Callahan, The Effects of

Vegetable Oil Properties on Injection and Combustion in Two Different Diesel Engines, *Ibid. 61*:1610–1619 (1984).
20. Murayama, T., Evaluating Vegetable Oils as a Diesel Fuel, *inform 5*:1138–1145 (1994).
21. Crookes, R.J., F. Kiannejad, and M.A.A. Nazha, Performance and Emissions of a 2.5 Litre Multi-cylinder Direct-Injection Automotive Diesel Engine with Alternative Diesel Fuels and Emulsions, in *IMechE Semin., Iss. 2: Fuels for Automot. and Ind. Diesel Engines*, Institute of Mechanical Engineers, London, 1993, pp. 151–159.
22. Crookes, R.J., F. Kiannejad, G. Sivalingam, and M.A.A. Nazha, Effects of Using Vegetable Oil Fuels and Their Emulsions on the Performance and Emissions of Single- and Multi-cylinder Diesel Engines, *Arch. Combust. 13*:57–74 (1993).
23. Crookes, R.J., M.A.A. Nazha, and F. Kiannejad, Single and Multi-cylinder Diesel-Engine Tests with Vegetable Oil Emulsions, SAE Tech. Paper Ser., Paper No. 922230, Society of Automotive Engineers, Warrendale, PA, 1992.
24. Ziejewski, M., and H.J. Goettler, Comparative Analysis of the Exhaust Emissions for Vegetable Oil Based Alternative Fuels, in SAE Spec. Publ. SP-900: Alternative Fuels for CI and SI Engines, Paper No. 920195, Society of Automotive Engineers, Warrendale, PA, 1992, pp. 65–73.
25. Ziejewski, M., H.J. Goettler, L.W. Cook, and J. Flicker, Polycyclic Aromatic Hydrocarbon Emissions from Plant Oil Based Alternative Fuels, SAE Tech. Paper Ser., Paper No. 911765, Society of Automotive Engineers, Warrendale, PA, 1991.
26. Mills, G.A., and A.G. Howard, A Preliminary Investigation of Polynuclear Aromatic Hydrocarbon Emissions from a Diesel Engine Operating on Vegetable Oil-Based Alternative Fuels, *J. Instit. Energy 56*:131–137 (1983).
27. Kesling, H.S., Jr., F.J. Liotta, and J.M. McFarland, Oxygenated Microemulsion Diesel Fuel, *ACS Fuel Chemistry Division Preprints 39*:322–326 (1994).
28. Schon, S.G., and E.A. Hazbun, Methanol as Cosurfactant for Microemulsions, U.S. Patent 5,004,479 (1991).
29. Schwab, A.W., and E.H. Pryde, Diesel Fuel–Aqueous Ethanol Microemulsions, U.S. Patent 4,451,265 (1984).
30. Boruff, P.A., A.W. Schwab, C.E. Goering, and E.H. Pryde, Evaluation of Diesel Fuel–Ethanol Microemulsions, *Trans. ASAE 25*:47–53 (1982).
31. ASTM D2500, Standard Test Method for Cloud Point of Petroleum Products, in *Annual Book of ASTM Standards*, Vol. 05.01, American Society for Testing and Materials, West Conshohocken, PA, 1991.
32. ASTM D97, Standard Test Method for Pour Point of Petroleum Products, in *Annual Book of ASTM Standards*, Vol. 05.02, American Society for Testing and Materials, West Conshohocken, PA, 1993.
33. ASTM D6371, Standard Test Method for Cold Filter Plugging Point of Diesel and Heating Fuels, in *Annual Book of ASTM Standards*, Vol. 05.04, American Society for Testing and Materials, West Conshohocken, PA, 1999.
34. ASTM D4539, Standard Test Method for Filterability of Diesel Fuels by Low-Temperature Flow Test, in *Annual Book of ASTM Standards*, Vol. 05.03, American Society for Testing and Materials, West Conshohocken, PA, 1994.

[Received December 7, 2001; accepted March 20, 2002]